

RSC Advances



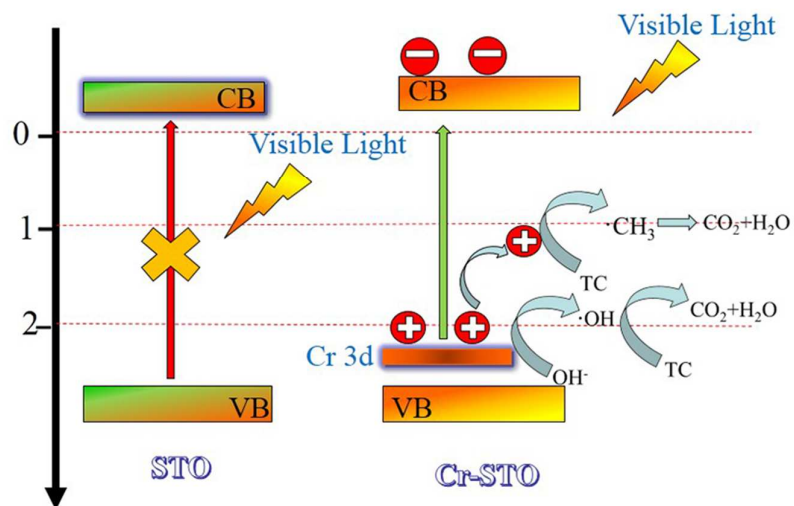
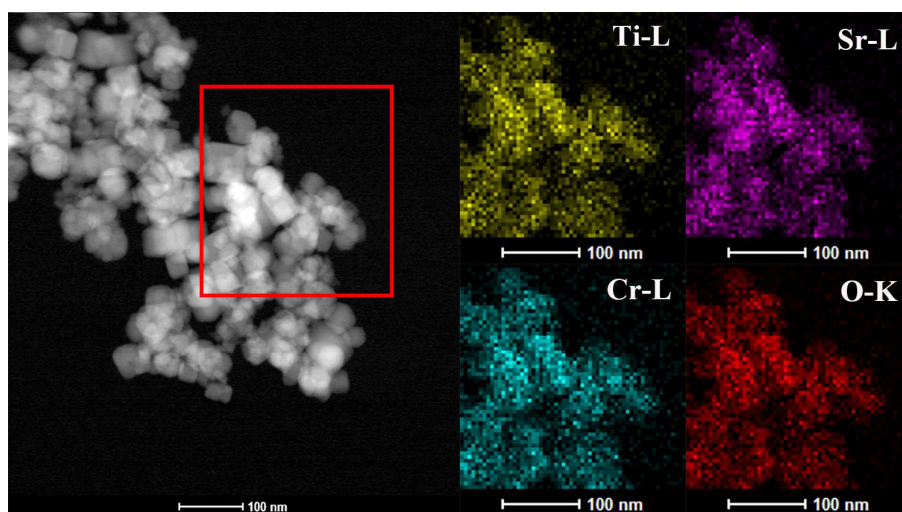
This is an *Accepted Manuscript*, which has been through the Royal Society of Chemistry peer review process and has been accepted for publication.

Accepted Manuscripts are published online shortly after acceptance, before technical editing, formatting and proof reading. Using this free service, authors can make their results available to the community, in citable form, before we publish the edited article. This *Accepted Manuscript* will be replaced by the edited, formatted and paginated article as soon as this is available.

You can find more information about *Accepted Manuscripts* in the [Information for Authors](#).

Please note that technical editing may introduce minor changes to the text and/or graphics, which may alter content. The journal's standard [Terms & Conditions](#) and the [Ethical guidelines](#) still apply. In no event shall the Royal Society of Chemistry be held responsible for any errors or omissions in this *Accepted Manuscript* or any consequences arising from the use of any information it contains.

TOC



Enhanced Visible-Light-Driven Photocatalytic Degradation of Tetracycline by Cr³⁺ Doping SrTiO₃ cubic Nanoparticles

Fanpeng Cai,^{a, b} Yubin Tang,^{a, *} Fangyan Chen,^a Yan Yan,^b Weidong Shi,^{b, *}

^a School of Biology and Chemical Engineering, Jiangsu University of Science and Technology, Zhenjiang, 212003, P. R. China.

^b School of Chemistry and Chemical Engineering, Jiangsu University, Zhenjiang, 212013, P. R. China.

**Corresponding author: Tel.: +86 511-85635850; Fax. : +86-511 85635859*

E-mail address: ybill@163.com (Y-b. Tang)

**Corresponding author: Tel.: +86 511 8879 0187; Fax. : +86 511 8879 1108*

E-mail address: swd1978@ujs.edu.cn (W. Shi)

Abstract:

The removal of Tetracyclines (TC), an extensively used antibiotics, from the environment has become a desiderate issue already. Recently, the photocatalytic oxidation on the surface of semiconductors provides a good tool for the degradation of TC, but most of them are UV-light driven rather than visible-light driven. Here, the Cr doping results in a large decrease of the band gap energy, making Cr³⁺ doped SrTiO₃ (Cr-STO) an attractive material for use as a visible-light-driven photocatalyst of tetracycline (TC) degradation. The photoactivity is improved upon the Cr/Sr weights ratio changing from 0.5% to 2%, and decreased when the Cr/Sr weights ratio changing from 3% to 10%. In this paper, we also explain the relationship between doping and photocatalytic activity. The existence of •OH radicals and holes were studied by electron spin resonance (ESR) spin-trap technique and trapping experiments.

Keywords: Tetracycline, Photocatalytic degradation, Hydrothermal method, Cr³⁺ doped SrTiO₃

1 Introduction

Tetracyclines (TC) are well-known antibiotics that have been extensively used in human and veterinary medicine to treat and prevent bacterial infections ¹. The existence of TC in water environments may cause serious threats to the ecosystem and human health by inducing proliferation of bacterial drug resistance. And thus, the removal of TC from the environment has become a desiderate issue already. As far as we know, the traditional physical and chemical treatments lack of adequate removal efficiency, and the new method tend to produce more harmful byproducts of biochemical treatment method. It is fortunately that the photocatalytic degradation processes provide a good tool for the transportation and degradation of TC. In the past few years, some research on the high-efficiency photocatalytic degradation of TC by semiconductor-based (such as TiO₂ and ZnO) photocatalysts have been reported ², but most of them are UV-light driven rather than visible-light driven. Therefore, new-type visible-light driven photocatalysts with high efficiency for TC degradation are still desired.

Strontium titanate (STO) has been regarded as one of the most promising photocatalysts for photocatalytic degradation of organic pollutants because of its strong catalytic activity, high chemical and photochemical stability and good biological compatibility ³⁻⁶. However, STO shows activities only under ultraviolet irradiation accounting for merely about 4% of the incoming solar energy, which limits its practical application. To overcome this defect, various approaches undertaken in the search for more-efficient and active photocatalysts for organic pollutants

degradation, the following approaches can be mentioned: doping, sensitization⁷⁻¹¹. Element doping is a good strategy that may create impurity energy levels within the band gap of the photocatalyst that facilitate absorption in the visible-light range¹²⁻¹⁵. The advantages of transition metal ion-doped STO is introduced in the crystal lattice defects, thus affecting the recombination of electrons and holes^{16,17}. Incorporation of certain metal ions can also extend the range of the wavelength of light absorbed¹⁸⁻²⁰. Recently, various cation or anion doped perovskite type compounds have been synthesized, and their corresponding activities under visible light have been investigated experimentally. It was reported that doping with metal atoms (M = Ru, Rh, Mn, Fe, Cr, Pb, and Ag) is an efficient method to improve the visible-light activity of STO²¹⁻²³. Herein, for the first time, we found Cr-STO cubic nanoparticles can function as visible-light-driven photocatalyst of TC degradation. To the best of our knowledge, none visible-light-driven photocatalysts of TC degradation, especially for Cr-STO, few reports of visible-light-driven photocatalysts for TC degradation were published.

In our work, a series of Cr-STO cubic nanoparticles with different Cr/Sr weights ratios were prepared by a one-pot hydrothermal method and used as photocatalysts for the degradation of TC. The photocatalytic activity of Cr-STO for TC degradation under visible light irradiation was obviously enhanced as compared to the pure STO. By the way, element Cr formed the chemical bonds rather than exists in the form of ions, which means the toxic element Cr turn into non-toxic after doped it into STO. The energy band gap can be precisely controlled from 3.2 eV to 2.55 eV by varying

the Cr/Sr weights ratio from 0 to 10 %. Moreover, the effects of the Cr/Sr weights ratio in the nanocomposites on the photocatalytic activity performance of TC degradation were investigated comparatively. The possible mechanism for the enhanced photocatalytic activity was also proposed based on the obtained experimental results.

2 Experimental section:

2.1 Chemicals

Titania TiO_2 (P25, TiO_2) was purchased from Degussa (Germany). $\text{Sr}(\text{OH})_2 \cdot 8\text{H}_2\text{O}$, KOH, $\text{Cr}(\text{NO})_3 \cdot 9\text{H}_2\text{O}$ and TC were purchased from Aladdin (China). All reagents were of analytical grade without further purification, and the deionized water was used in all experiments.

2.2 Synthesis of pure STO and Cr-STO cubic nanoparticles

Pure STO cubic nanoparticles were synthesized through hydrothermal reaction: 0.847 g $\text{Sr}(\text{OH})_2 \cdot 8\text{H}_2\text{O}$, 0.3 g TiO_2 powders and 2.1 g KOH were dissolved in 35 mL purified water. After stirred for about 30 min, the as-obtained mixture was transferred into a Teflon-lined stainless steel autoclave of 50.0 mL capacity. The hydrothermal route was carried out at 150 °C for 72 h in stainless steel tank. After the hydrothermal treatment the product was naturally cooled down to room temperature in the vessel and was washed with deionized water by repeated centrifugation until pH of the supernatant liquid down to less than 8, and the production were dried at 60 °C in air. Cr-STO cubic nanoparticles were prepared by the same method with an extra reagent of $\text{Cr}(\text{NO})_3 \cdot 9\text{H}_2\text{O}$ introduce in the STO precursors liquid. Obtained samples with Cr/Sr weight ratio of 0, 0.5%, 1%, 2%, 3%, 5% and 10% were labeled as sample STO,

Cr0.5, Cr1, Cr2, Cr3, Cr5 and Cr10.

2.3 Characterization

Powder X-ray diffraction (XRD) patterns were obtained on a D/MAX-2500 diffractometer (Rigaku, Japan) using a Cu K α radiation source ($\lambda = 1.54056 \text{ \AA}$) at a scan rate of 7° min^{-1} to determine the crystal phase of obtained samples. Transmission electron microscopy (TEM), high-resolution transmission electron microscopy (HRTEM) and HAADF-STEM mapping analyses were collected on an F20 S-TWIN electron microscope (Tecnai G2, FEI Co.), using a 200 kV accelerating voltage. Uv-vis absorption spectra of samples were measured by using UV-vis spectrometer (Shinadzu UV-2500). X-ray photoelectron spectroscopy (XPS) data were obtained by an ESCALa-b220i-XL electron spectrometer (VGScientific, England) using 300 W Al K α radiation. ESR experiments were conducted with a Bruker EPR ELEXSYS 500 spectrometer equipped with an in situ irradiation source (a Quanta-Ray Nd:YAG laser system with $\lambda=532 \text{ nm}$). The same quartz tube was used for all the measurements to minimize errors.

2.4 Photocatalytic degradation of TC.

The photocatalytic activities of Cr-STO were evaluated by the degradation of TC in aqueous solution under visible light irradiation of a 250W xenon lamp with the 420 nm cutoff filter. In a typical procedure, 0.1 g of pure STO or Cr-STO samples were dissolved in 100 mL of 10 mg/L TC solution. In order to eliminate the adsorption effect, the reactor was kept in darkness for 30 min to reach adsorption-desorption equilibrium. The photochemical reactor was irradiated with a 250 W xenon lamp

which was located with a distance of 8 cm at one side of the containing solution. During the irradiation procedure, the reaction sample was collected at 10-min intervals and centrifuged to remove photocatalyst particles. The photocatalytic degradation ratio (DR) was calculated by the following formula:

$$DR\% = \left(1 - \frac{A_i}{A_0}\right) \times 100\% \quad (1)$$

Here A_0 is the initial absorbance of TC that reached adsorption-desorption equilibrium, while A_i is the absorbance after the sampling analysis. The concentration was analyzed by measuring the maximum absorbance at 357 nm for TC using a UV-vis spectrophotometer.

3 Results and discussion

3.1 Morphology and structure

The crystallographic structure and phase purity of the as-prepared samples were examined by X-ray powder diffraction (XRD). A typical XRD pattern recorded from the all samples are shown in Fig. 1a. XRD patterns revealed that the prepared samples maintained a STO crystalline structure (JCPDS card no. 05-0634) after Cr^{3+} doping (Fig. 1a). It clearly shows that Cr^{3+} doped into the lattice of STO did not affect the structure of STO, even in the high content of 10 wt% Cr. Fig. 1b shows a magnified image of the diffraction peaks for the (110) plane. The positions of the diffraction peak tended to shift to higher angles by the doping of Cr ions as shown in Fig. 1b, which confirmed the incorporation of the Cr ions into the STO crystal lattice^{24, 25}.

The morphology and size of as-synthesized Cr₂ products were studied by TEM and HRTEM analyses (Fig. 2). According to TEM images (Fig 2a and 2b), it can be

seen that the Cr₂ consist of large numbers of uniform cubic nanocrystals. The diameters of the individual cubic nanocrystals are 50 nm. HRTEM images (Fig. 2c and Fig. 2d) show the representative individual nanocrystal. The clear lattice fringes indicate the obtained Cr₂ nanocrystals were well-crystallized. Distinct interplanar spacing of 0.27 nm is ascribed to the (110) crystalline plane of cubic phase of STO (JCPDS card no. 05-0634). The inset of Fig. 2d shows the fast Fourier transform (FFT) pattern related to a single particle, which clearly demonstrate that Cr₂ was presented in a single-crystal phase as shown by the separated electron diffraction spots.

The high-angle annular dark-field scanning TEM (HAADF-STEM) image of Cr₂ photocatalyst is shown in Fig. 3 (left), Cr-STO cubic nanoparticles can be clearly observed with distinct color contrast. The element distribution maps of Cr-L, Ti-L, Sr-L and O-K are also given in Fig. 3 and well-defined with sharp contrast. Moreover, the elemental mapping demonstrates that the Cr-L, Ti-L, Sr-L and O-K signals are exhibit the same shape within the Cr-STO sample, demonstrating the certain existence of Sr-Cr-Ti-O composite in the sample.

The valence band (VB) top of STO is lifted up by the occupied Cr³⁺ level, while the original conduction band (CB) bottom determined by Ti 3d orbital is hardly affected¹⁶. Under visible-light illumination, the photogenerated electrons on Cr-STO are photoexcited from the VB (Cr 3d) to the CB (Ti 3d). The occupied Cr³⁺ level is about 1.0 eV higher than the VB top formed by Ti 3d¹⁹. Therefore, the band gap for the Cr-STO becomes smaller. In order to obtain the oxidation state of Cr, we carried out XPS measurement (Fig. 4). In the Cr 2p spectrum of Cr-STO (Fig. 4b), only one

sharp peak is observed at 575.57 eV, which could be assigned to Cr³⁺. No other XPS peaks, for example, Cr⁶⁺ (580.2 eV) were observed. These results clearly show that Cr³⁺ ions are successfully incorporated into the lattice of STO.

3.2 UV-vis absorption spectra

As shown in the UV-vis absorption spectra (Fig. 5) of all samples, pure STO has the absorption edge at about 400 nm, which is correspond to the UV light region. After Cr³⁺ doping, the visible-light-response of Cr³⁺ doped STO samples were largely enhanced with red-shifted light absorptions. Particularly, the absorption intensity at around 420 nm was dramatically enhanced after Cr³⁺ doping. Energy band gap (E_g) was calculated using the following relation²⁶⁻²⁹:

$$\alpha = \frac{A(h\nu - E_g)^n}{h\nu} \quad (2)$$

Where A and n are constant, and the n equal to 1/2 for direct band gap semiconductors. The estimated band gaps from the plots of $(\alpha h\nu)^2$ versus $h\nu$ are shown in Fig. 5b and Table 1, from which we can find that the energy band gap is decreased from 3.2 eV to 2.55 eV as the Cr³⁺ doping amount increased from 0 to 10%. After doping, the Cr 3d levels are inserted into the original band gap of STO, which induces an obvious absorption in the visible-light region¹⁹.

3.3 Photocatalytic Degradation of TC

The photocatalytic degradation experiments were conducted under visible light ($\lambda > 420$ nm). In our case, we found the as-prepared Cr-STO cubic nanoparticles had extraordinary visible-light-driven photocatalytic activity for the degradation of TC. The contrast experiments on the catalytic activity of the Cr-STO cubic nanoparticles,

pure STO cubic nanoparticles under visible light irradiation were carried out. Fig. 6a displays the time-resolved of the UV-vis spectra during the photodegradation of TC mediated by Cr₂ sample under visible light illumination ($\lambda > 420$ nm). A rapid decrease of TC absorption at wavelength of 357 nm was observed, accompanied with an absorption band shift to the shorter wavelength, indicating the degradation of TC. As can be seen from the above spectra, absorption of Cr₂ suspensions gradually decreased during photodegradation. As compared, the test of degradation of TC solution without photocatalyst under visible light was conducted. The result was shown in Fig. 6b, there is almost no degradation. In addition, the major absorption peak corresponding to TC was shifted from 357 to 350 nm step by step, indicating the removal of benzene functional groups one by one. The sharp decrease and shift of the major absorption band within 60 mins indicate that the Cr₂ sample exhibits excellent photocatalytic activity on degradation of TC due to its suitable VB, which is made up predominately of the Cr 3d state.

The corresponding plots for the concentration changes of TC determined from its characteristic absorption peak (at 357 nm) are shown in Fig. 6b and the degradation ratios of all samples list in the Table 1. Cr₂ shows the maximum activity for photocatalytic of TC degradation. In details, the photocatalytic activity showing an upward trend from Cr_{0.5} to Cr₂ sample. With the increased of doping amount, the photocatalytic activity present a downward trend for the next state. Nevertheless, all the Cr-STO composites showed better photocatalytic activity than the pure STO. In spite of the narrower band gaps, the photocatalytic activity for the degradation of TC

by sample Cr3-Cr10 was lower than that of sample Cr2. It is reasonable because the oxidative potential is also reduced as the energy band gap decreased, which means the band gap is not the narrower the better³⁰.

3.4 Kinetic Study

Fig. 7 shows the approximate linear relationship of $\ln(C_0/C)$ versus irradiation time t for all samples, which indicates the photocatalytic degradation process of TC can be considered as a Langmuir-Hinshelwood first-order kinetics reaction due to the low concentration of the substrate³¹⁻³³. Its kinetics can be expressed as follows: $\ln(C_0/C) = K_{app}t$, where K_{app} is the degradation reaction rate constant, C_0 and C are the initial concentration and the concentration at reaction time t for TC, respectively. The apparent decomposition rates constant K_{app} values for all samples are given in Table 3. It is obvious that the Cr2 sample with the largest rate constant ($K_{app} = 0.01607 \text{ min}^{-1}$) has the highest catalytic activity, and further confirm the conclusion that the visible light-induced photocatalytic activity resulted from Fig. 6. Experimental evidence for all the photocatalytic degradation in this work suggests that Cr-STO was an excellent visible-light-driven photocatalyst of TC degradation.

3.5 ESR study

The photocatalytic mechanism was studied by ESR spin-trap technique and trapping experiments of radicals and holes³⁴⁻³⁹. ESR spin-trap technique (with DMPO) was employed to monitor the reactive oxygen species generated during the irradiation of the present system, the result was shown in Fig. 8. A Nd:YAG laser ($\lambda = 532 \text{ nm}$) was employed to irradiate catalysts containing suspensions. As depicted in the Fig. 8a,

four characteristic peaks of DMPO-•OH (marked with ★) and six characteristic peaks of DMPO-•CH₃ (marked with ※) were clearly observed in the suspension of Cr-STO cubic nanoparticles at the instant of light on, and their intensity increased with irradiation time. No such signals were detected when the suspension were kept in darkness. This means that irradiation is essential to the generation of •OH and •CH₃ on the surface of the catalyst. The evidence that DMPO-•OH and DMPO-•CH₃ are produced on the surface of visible illuminated Cr-STO provides a solid indication that the photocatalyst can be efficiently excited by visible light to create electron hole pairs and that the charge separation is maintained long enough to react with adsorbed TC/H₂O and to produce a series of active •OH and •CH₃ radicals which finally induce the decomposition of TC. Therefore, a dual mechanism involving both •OH radicals and •CH₃ radicals oxidation is expected in the photocatalysis process. Meanwhile, the active species in the present photocatalytic oxidation were examined by observing the reaction process under different conditions. In order to confirm this result, we provide the ESR irradiate without catalysts in water, and the figure was shown in Fig. S1. As can be seen from the figure, the characteristic peaks of DMPO-•OH and DMPO-•CH₃ cannot be observed in the absence of Cr-STO either in dark or in visible light irradiation. Fig. 8b shows the photocatalytic degradation of TC with the addition of holes and •OH radical scavengers, respectively. The addition of tert-butanol as •OH radicals scavenger caused a decrease of the photocatalytic degradation of TC, meanwhile the TC also could be hardly degraded with the addition of capture for holes (EDTA-Na), suggesting that the •OH radicals and direct hole oxidation mainly

govern the photocatalytic process in the photocatalytic degradation of TC.

The reaction mechanism is thus briefly described in Fig. 9. Under visible light irradiation, electrons in the VB of Cr 3d orbit are excited into the CB, leaving holes in the VB^{16, 40}. And then the holes that travel to the surface of the Cr-STO and react with adsorbed H₂O, OH⁻ and TC to produce •OH and •CH₃ radicals which finally induce the decomposition of organic compounds. Combine with the trapping experiments of radicals and holes, •OH radicals and holes play a crucial role for the degradation of TC. It can be concluded that h⁺ and •OH radicals are the main active species of Cr-STO cubic nanoparticles in aqueous solution under visible-light irradiation.

4 Conclusions

In conclusion, we have developed a facile one-pot hydrothermal method to synthesize Cr-STO cubic nanoparticles with uniform morphology. The resulting Cr-STO cubic nanoparticles exhibit enhanced photocatalytic activity for the degradation of TC under visible light. Moreover, we concluded that h⁺ and •OH radicals are the main active species of Cr-STO cubic nanoparticles in aqueous solution under visible-light irradiation by ESR spin-trap technique and trapping experiments of radicals and holes.

ACKNOWLEDGMENT

We gratefully acknowledge the financial support of the National Natural Science Foundation of China (21276116, 21477050, 21301076 and 21303074), Excellent Youth Foundation of Jiangsu Nature Scientific Committee (BK20140011), Program for high-level innovative and entrepreneurial talents in Jiangsu Province, Program for

New Century Excellent Talents in University (NCET-13-0835), Henry Fok Education Foundation (141068) and Six Talents Peak Project in Jiangsu Province (XCL-025).

References

1. C. Reyes, J. Fernández, J. Freer, M. A. Mondaca, C. Zaror, S. Malato and H. D. Mansilla, *Journal of Photochemistry and Photobiology A: Chemistry*, 2006, **184**, 141-146.
2. R. A. Palominos, M. A. Mondaca, A. Giraldo, G. Peñuela, M. Pérez-Moya and H. D. Mansilla, *Catalysis Today*, 2009, **144**, 100-105.
3. X. Yuan, M. Zheng, Y. Zhang, T. Zhou, C. Li, X. Fang, L. Ma and W. Shen, *Inorganic chemistry*, 2013, **52**, 2581-2587.
4. Q. Kuang and S. Yang, *ACS applied materials & interfaces*, 2013, **5**, 3683-3690.
5. A. E. Souza, G. T. A. Santos, B. C. Barra, W. D. Macedo, S. R. Teixeira, C. M. Santos, A. M. O. R. Senos, L. Amaral and E. Longo, *Crystal Growth & Design*, 2012, **12**, 5671-5679.
6. F. A. Rabuffetti, P. C. Stair and K. R. Poeppelmeier, *The Journal of Physical Chemistry C*, 2010, **114**, 11056-11067.
7. H. Hussain, X. Torrelles, P. Rajput, M. Nicotra, G. Thornton and J. Zegenhagen, *The Journal of Physical Chemistry C*, 2014, **118**, 10980-10988.
8. J. S. Jeong, P. Ambwani, B. Jalan, C. Leighton and K. A. Mkhoyan, *ACS nano*, 2013, **7**, 4487-4494.
9. J. A. Enterkin, W. Setthapun, J. W. Elam, S. T. Christensen, F. A. Rabuffetti, L. D. Marks, P. C. Stair, K. R. Poeppelmeier and C. L. Marshall, *ACS Catalysis*, 2011, **1**, 629-635.
10. H. Yu, H. Irie, Y. Shimodaira, Y. Hosogi, Y. Kuroda, M. Miyauchi and K. Hashimoto, *The Journal of Physical Chemistry C*, 2010, **114**, 16481-16487.
11. M. Liu, X. Qiu, M. Miyauchi and K. Hashimoto, *Journal of the American Chemical Society*, 2013, **135**, 10064-10072.
12. H.-C. Chen, C.-W. Huang, J. C. S. Wu and S.-T. Lin, *The Journal of Physical Chemistry C*, 2012, **116**, 7897-7903.
13. X. Zhou, J. Shi and C. Li, *The Journal of Physical Chemistry C*, 2011, **115**, 8305-8311.
14. Y. Wang, H. Xu, X. Wang, X. Zhang, H. Jia, L. Zhang and J. Qiu, *The journal of physical chemistry. B*, 2006, **110**, 13835-13840.
15. R. Kenta, T. Ishii, H. Kato and A. Kudo, *The Journal of Physical Chemistry B*, 2004, **108**, 8992-8995.
16. J. Wang, T. Fang, S. Yan, Z. Li, T. Yu and Z. Zou, *Computational Materials Science*, 2013, **79**, 87-94.
17. I. Bykov, M. Makarova, V. Trepakov, A. Dejneka, L. Yurchenko, L. Yurchenko, A. Jäger and L. Jastrabik, *physica status solidi (b)*, 2013, **250**, 821-824.
18. U. Sulaeman, S. Yin and T. Sato, *Applied Catalysis B: Environmental*, 2011, **105**, 206-210.
19. H. Li, S. Yin, Y. Wang, T. Sekino, S. W. Lee and T. Sato, *Journal of Catalysis*, 2013, **297**, 65-69.
20. Z. Jiao, Y. Zhang, T. Chen, Q. Dong, G. Lu and Y. Bi, *Chemistry*, 2014, **20**, 2654-2662.
21. K. Maeda, *ACS applied materials & interfaces*, 2014, **6**, 2167-2173.
22. S. Kawasaki, K. Akagi, K. Nakatsuji, S. Yamamoto, I. Matsuda, Y. Harada, J. Yoshinobu, F. Komori, R. Takahashi, M. Lippmaa, C. Sakai, H. Niwa, M. Oshima, K. Iwashina and A. Kudo, *The Journal of Physical Chemistry C*, 2012, **116**, 24445-24448.
23. H. Irie, Y. Maruyama and K. Hashimoto, *Journal of Physical Chemistry C*, 2007, **111**, 1847-1852.

24. D. Wang, J. Ye, T. Kako and T. Kimura, *The journal of physical chemistry. B*, 2006, **110**, 15824-15830.
25. H. W. Kang, S. N. Lim, D. Song and S. B. Park, *International Journal of Hydrogen Energy*, 2012, **37**, 11602-11610.
26. J. H. Nobbs, *Review of Progress in Coloration and Related Topics*, 1985, **15**, 66-75.
27. R. Hu, Y. Wang, Y. Zou, X. Chen, S. Liu and X. Luo, *Journal of Applied Physics*, 2013, **113**, 063108.
28. D. Mitoraj and H. Kisch, *The Journal of Physical Chemistry C*, 2009, **113**, 20890-20895.
29. C. Sandoval and A. D. Kim, *Journal of the Optical Society of America. A, Optics, image science, and vision*, 2014, **31**, 628-636.
30. P. Reunchan, N. Umezawa, S. Ouyang and J. Ye, *Physical Chemistry Chemical Physics*, 2012, **14**, 1876.
31. C. Zhao, M. Pelaez, X. Duan, H. Deng, K. O'Shea, D. Fatta-Kassinos and D. D. Dionysiou, *Applied Catalysis B: Environmental*, 2013, **134-135**, 83-92.
32. S. Valencia, F. Cataño, L. Rios, G. Restrepo and J. Marín, *Applied Catalysis B: Environmental*, 2011, **104**, 300-304.
33. E. Du, Y. X. Zhang and L. Zheng, *Reaction Kinetics and Catalysis Letters*, 2009, **97**, 83-90.
34. W. Zhao, W. Ma, C. Chen, J. Zhao and Z. Shuai, *Journal of the American Chemical Society*, 2004, **126**, 4782-4783.
35. C. Wang, H. Zhang, F. Li and L. Zhu, *Environmental science & technology*, 2010, **44**, 6843-6848.
36. Z. Wang, W. Ma, C. Chen, H. Ji and J. Zhao, *Chemical Engineering Journal*, 2011, **170**, 353-362.
37. T. Xu, L. Zhang, H. Cheng and Y. Zhu, *Applied Catalysis B: Environmental*, 2011, **101**, 382-387.
38. Y. Yang and S. Mu, *The Journal of Physical Chemistry C*, 2011, **115**, 18721-18728.
39. D. V. Azamat, A. Dejneka, J. Lančok, L. Jastrabik, V. A. Trepakov, Z. Brykнар, E. V. Neverova and A. G. Badalyan, *Journal of Physics and Chemistry of Solids*, 2014, **75**, 271-275.
40. H. Yu, J. Wang, S. Yan, T. Yu and Z. Zou, *Journal of Photochemistry and Photobiology A: Chemistry*, 2014, **275**, 65-71.

Table 1

Information of all samples used in experiments, including calculated direct band gap energy, degradation ratio and apparent rate constant values.

Samples	STO	Cr0.5	Cr1	Cr2	Cr3	Cr5	Cr10
E _g (eV)	3.20	3.00	2.91	2.71	2.65	2.55	2.65
DRs	6%	55%	65%	68%	55%	50%	39%
K _{app} (min ⁻¹)	~	0.0117	0.01412	0.01607	0.01397	0.01135	0.00843

Figure captions:

Fig. 1. (a) XRD patterns of pure STO and Cr-STO: a-pure STO, b-Cr0.5, c-Cr1, d-Cr2, e-Cr3, f-Cr5 and g-Cr10. (b) the magnified XRD patterns in the range of $2\theta=31^\circ$ to 34° of STO and Cr10.

Fig. 2. (a, b) TEM images of Cr2. (c) HRTEM image and (d) the magnified HRTEM image from (c). Inset in (d) shows the FFT pattern related to a single particle.

Fig. 3. HAADF-STEM image of sample Cr2 and maps of Ti-L, Sr-L, Cr-L and O-K demonstrating the spatial distribution of Ti, Sr, Cr and O elements.

Fig. 4. The full range XPS spectrum (a) and the high-resolution XPS spectrum of Cr 2p3 (b) of Cr2 sample.

Fig. 5. (a) UV-vis absorption spectra, (b) calculated direct band gap energy of different pure STO and Cr-STO samples.

Fig. 6. (a) The temporal evolution of the spectra during the photodegradation of TC mediated by Cr2 under visible light. (b) The degradation ratio of different samples in 60 min.

Fig. 7. Kinetics of the photocatalytic degradation of (a) Cr0.5 (b) Cr1, (c) Cr2, (d) Cr3, (e) Cr5 and (f) Cr10 under visible light in 60 min.

Fig. 8. (a) DMPO spin-trapping ESR spectra of Cr-STO cubic nanoparticles. (b) Photocatalytic degradation of TC with the addition of holes and radical scavenger.

Fig. 9. A plausible mechanism of photocatalytic of electrons and holes under visible light illumination on Cr-STO photocatalysts.

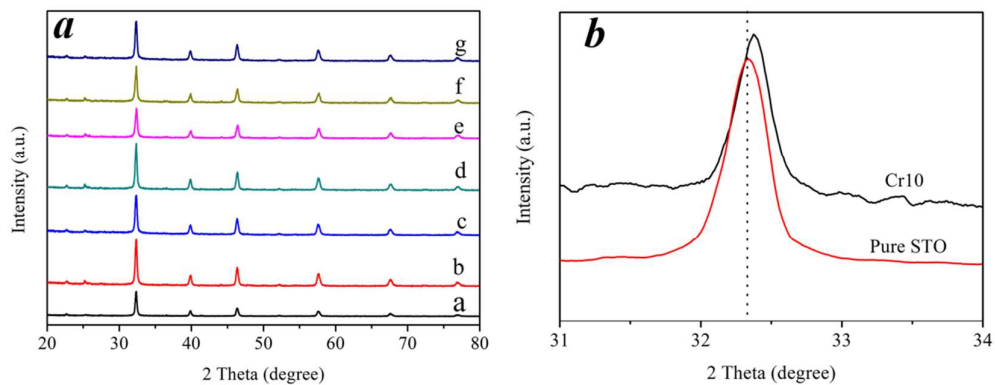


Fig. 1. (a) XRD patterns of pure STO and Cr-STO: a-pure STO, b-Cr0.5, c-Cr1, d-Cr2, e-Cr3, f-Cr5 and g-Cr10. (b) the magnified XRD patterns in the range of $2\theta=31^\circ$ to 34° of STO and Cr10.

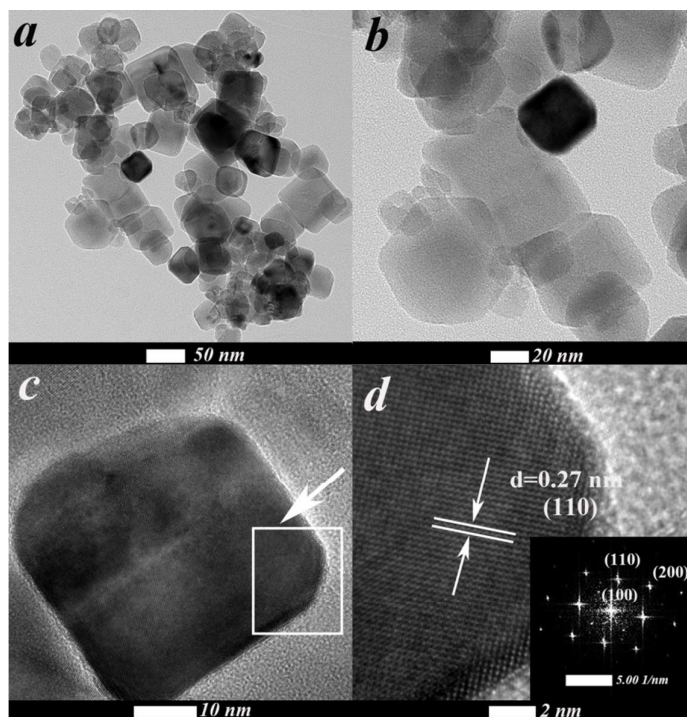


Fig. 2. (a, b) TEM images of Cr₂. (c) HRTEM image and (d) the magnified HRTEM image from (c). Inset in (d) shows the FFT pattern related to a single particle.

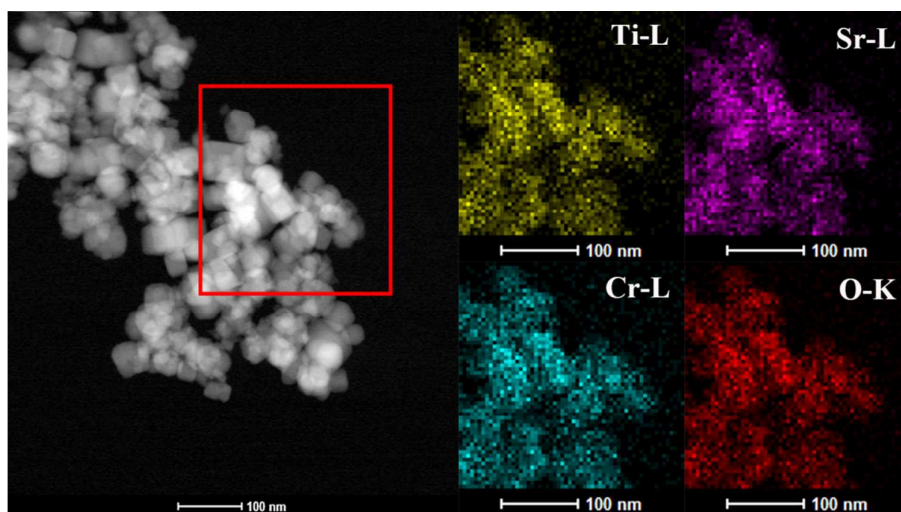


Fig. 3. HAADF-STEM image of sample Cr2 and maps of Ti-L, Sr-L, Cr-L and O-K

demonstrating the spatial distribution of Ti, Sr, Cr and O elements.

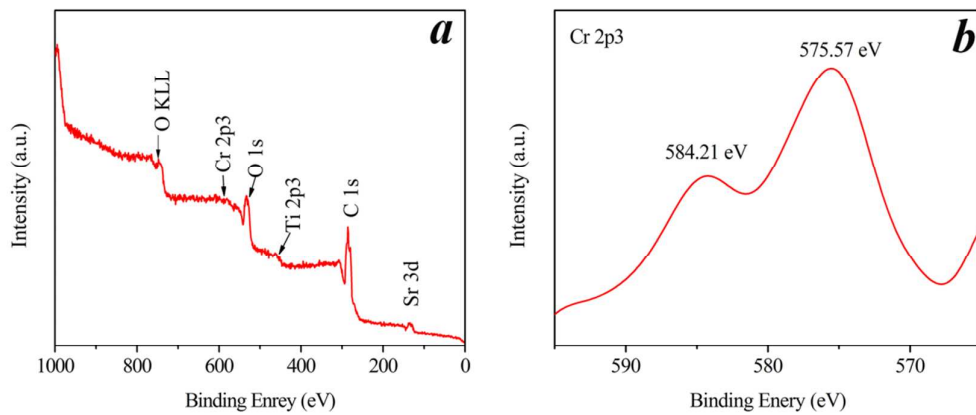


Fig. 4. The full range XPS spectrum (a) and the high-resolution XPS spectrum of Cr 2p3 (b) of Cr₂ sample.

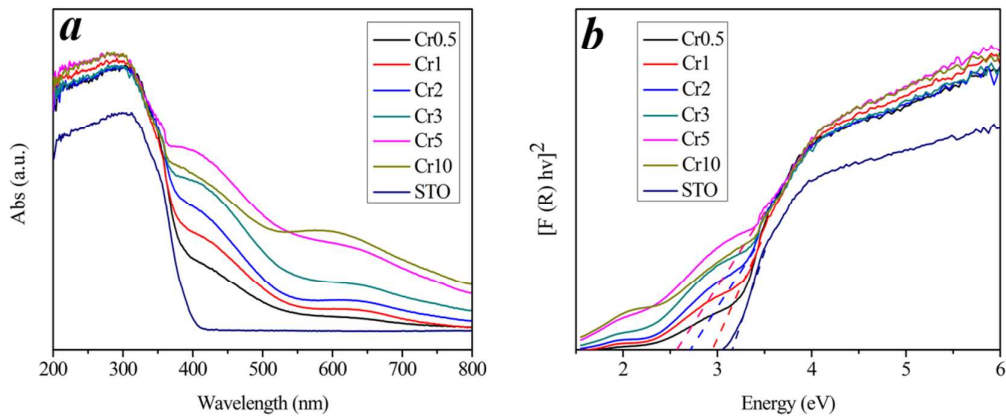


Fig. 5. (a) UV-vis absorption spectra, (b) calculated direct band gap energy of different pure STO and Cr-STO samples.

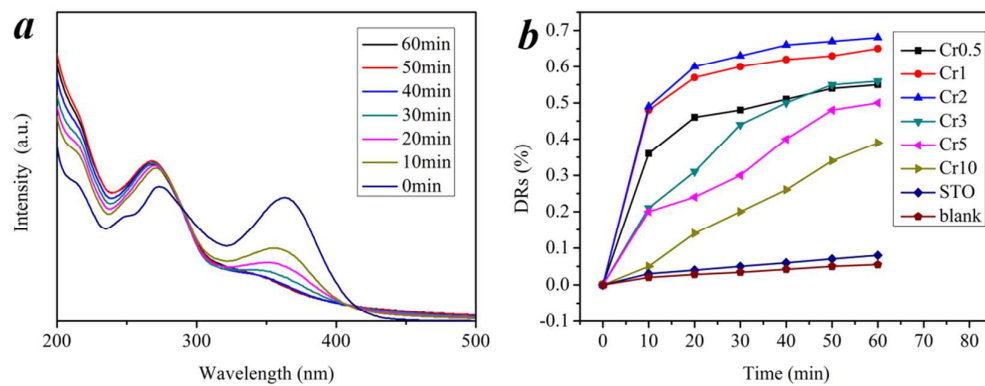


Fig. 6. (a) The temporal evolution of the spectra during the photodegradation of TC mediated by Cr2 under visible light. (b) The degradation ratio of different samples in 60 min.

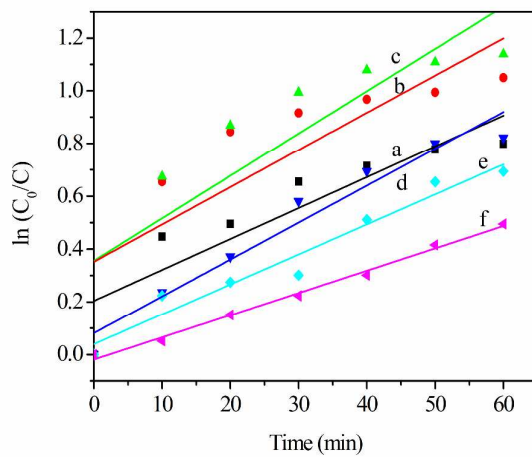


Fig. 7. Kinetics of the photocatalytic degradation of (a) Cr0.5 (b) Cr1, (c) Cr2, (d) Cr3, (e) Cr5 and (f) Cr10 under visible light in 60 min.

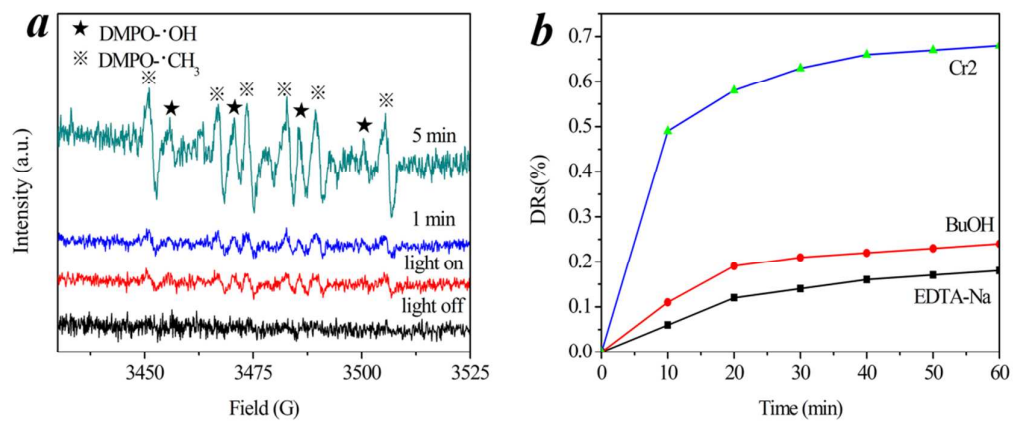


Fig. 8. (a) DMPO spin-trapping ESR spectra of Cr-STO cubic nanoparticles. (b) Photocatalytic degradation of TC with the addition of holes and radical scavenger.

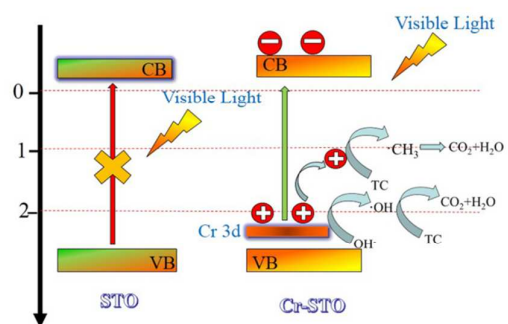


Fig. 9. A plausible mechanism of photocatalytic of electrons and holes under visible light illumination on Cr-STO photocatalysts.